


Lamellar Morphology of Disorder α' -Crystals of Poly(L-Lactic Acid)

Katalee Jariyavidyanont, Andreas Janke, Qiang Yu, Thomas Thurn-Albrecht, and René Androsch*

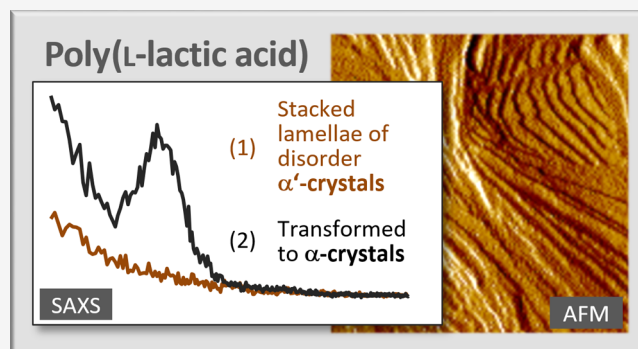
Cite This: *Cryst. Growth Des.* 2024, 24, 1825–1834

Read Online

ACCESS |

 Metrics & More Article Recommendations

ABSTRACT: Crystallization of poly(L-lactic acid) (PLLA) at temperatures lower and higher than about 100–120 °C leads to the formation of α' - and α -crystals, respectively. Related to the formation of different crystal polymorphs after crystallization at different temperatures, the small-angle X-ray scattering (SAXS) patterns only show a long-period maximum after crystallization at high temperatures, when α -crystals are present. Reason for the absence of a long-period peak after low-temperature crystallization is insufficient density contrast between the formed α' -crystals and the amorphous phase but not the absence of lamellar stacks and long-range periodicity. This conclusion is based on the observation of a long period after the transformation of α' -crystals of rather low density into α -crystals of higher density, by thermal treatment, while keeping the semicrystalline morphology quasi-unchanged. Long-range periodicity and formation of lamellae in PLLA containing α' -crystals are ultimately proven by atomic force microscopy, despite a long period is not detected by SAXS.



INTRODUCTION

Poly(L-lactic acid) (PLLA) is an environment-friendly polymer of increasing economic importance since it is produced from short-term renewable resources and since it is biodegradable.^{1–3} Many of its properties are controlled by the presence of crystals which, for example, provide mechanical stability^{4,5} at temperatures higher than the glass transition temperature T_g of around 60 °C.^{6,7} Typically, it is processed by conventional technologies, such as extrusion or injection molding, involving cooling the melt while shaping it.

As a function of the conditions of solidification, different supermolecular structures can be obtained. These include the fully amorphous state when cooling the melt faster than about 1 K/s to below T_g ,^{8–10} disorder α' -crystals when crystallizing the melt at temperatures lower than about 100–120 °C, and α -crystals when crystallizing at higher temperatures.^{11–13} While α -crystals are consistently described as exhibiting an orthorhombic symmetry,^{14–16} the unit cell of α' -crystals is either orthorhombic^{16,17} or pseudo-hexagonal.^{18,19} In the latter crystal polymorph, the distances between neighbored molecular stems are slightly larger than in the α -phase, and the helical chains contain conformational defects/distortions.^{18–20} These defects then also cause a decrease in the thermal stability/melting temperature and enthalpy of melting, affecting all material properties.^{21–25} Crystallization of both crystal forms occurs spherulitically;²⁶ however, information about the morphology and organization/spatial arrangement of α' -crystals beyond conclusions, which may be derived from the spherulitic growth, is not available yet.

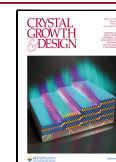
For PLLA, crystallized at a relatively high temperature, growth of lamellae is well evidenced by direct imaging using transmission electron microscopy (TEM)²⁷ or atomic force microscopy (AFM),²⁸ and by small-angle X-ray scattering (SAXS).^{29–33} Important in the context of the present study regarding SAXS analysis of the semicrystalline morphology, a long-period maximum, which typically shows up in the scattering signal as a result of the formation of lamellar stacks,^{34–36} is only observed on crystallization at temperatures higher than about 100 °C, while it is absent on crystallization at lower temperatures, when α' -crystals are present;^{29–33} only in few studies has a SAXS long-period maximum been reported after low-temperature crystallization.^{18,36} Within studies of the transition of α' - into α -crystals on heating,^{18,37} it was suggested that the absence, or at least strong weakening of the long-period maximum after crystallization at low temperature is caused by the lower density of α' -crystals compared to that of α -crystals,^{15,17,38} causing a reduced electron-density contrast between the amorphous and ordered phases,^{15,17,38,39} but that it is not caused by the absence of lamellae. Reports of the density of α -crystals include values of 1.29, 1.285, or 1.262 g/cm³, while for α' -crystals, a density of 1.250 g/cm³ is suggested.^{38–40} With a

Received: December 16, 2023

Revised: January 17, 2024

Accepted: January 18, 2024

Published: February 5, 2024



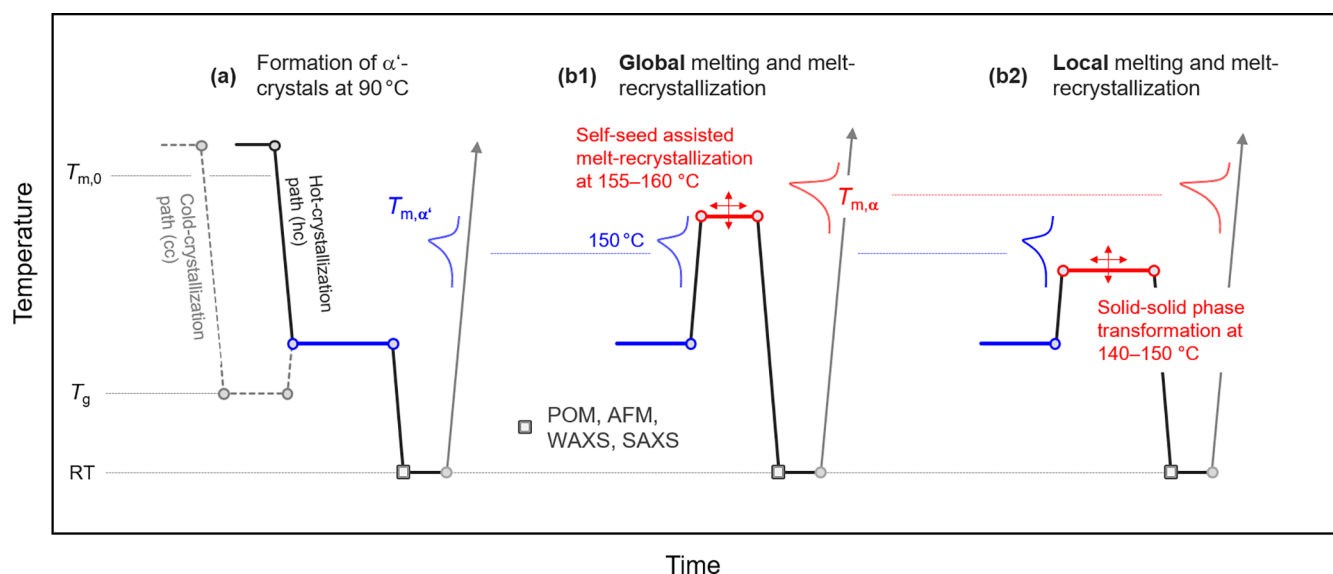


Figure 1. Thermal pathways for generation of PLLA containing α' -crystals [path (a), left] and PLLA containing α -crystals formed by reorganization of the initial structure/ α' -crystals at elevated temperature [paths (b1) and (b2)], before their analysis at room temperature (RT) (see square symbols). Blue and red coloring of isothermal segments indicates the formation of α' - and α -crystals, respectively, with their (different) melting temperatures sketched with the shown melting peaks. Further explanations are provided in the text.

density of the amorphous phase of 1.248 g/cm³, measured using a completely amorphous D/L-poly lactide,³⁹ the density difference between the amorphous phase and α' -crystals is negligible, and also in the presence of α -crystals, the density difference is rather low.

To date, to the best of our knowledge, the formation of lamellae in the temperature range of the formation of disordered α' -crystals has not yet been proven by direct imaging/microscopy, which is therefore the main subject of the present work. The above-described suggestion that the absence of a long-period maximum is indeed caused by low-density contrast between the amorphous and crystalline phases is then attempted to be proven by converting the lower density α' -crystals into higher density α -crystals without a qualitative change in the semicrystalline morphology and observation of the SAXS patterns – all measured at an identical temperature of about 20 °C, and therefore ruling out temperature-induced changes of the density contrast – before and after the α'/α -phase transformation. This experiment then enhances/completes an earlier study in which the α'/α -phase transformation and its effect on the SAXS curves were measured on heating.¹⁸

This paper is structured such that in the first part, thermal profiles for the generation of α' -crystals and their transformation to α -crystals are explained, including the presentation of wide-angle X-ray scattering (WAXS) data as an evidence for the prevalence of the specific crystal polymorphs, before and after phase transition. This is followed, in the second part, by providing information about the semicrystalline morphology of PLLA containing α' -crystals as well as α -crystals generated by reorganization of α' -crystals using microscopy. In the third part of this work, the corresponding SAXS patterns are presented and discussed. It is worth noting that to ensure well-defined crystallization/recrystallization pathways, measurements were performed on both micrometer-scale samples prepared in a fast scanning chip calorimeter (FSC) and samples thermally treated in a conventional differential scanning calorimeter (DSC).

EXPERIMENTAL SECTION

Materials and Initial Preparation. Extrusion-grade PLLA homopolymers with mass-average molar masses of 117 and 120 kg/mol and D-isomer contents lower than 1% were provided by Sulzer Chemtec Ltd. (Switzerland)^{41,42} and Total Corbion (The Netherlands),⁴³ respectively. Both polymers were delivered as pellets and used equivalently across the entire study. The preparation of FSC samples for subsequent structural analyses included microtoming of sections with a thickness of 10–20 μm and afterward reduction of their lateral dimensions to about 300 μm , with the rather large sample size facilitating in particular X-ray analyses. Films of 220 μm thickness were prepared with a film-maker accessory (Specac Ltd., Orpington, UK) and a heatable hydraulic press (LOT QD, Darmstadt, Germany) for obtaining flat samples for subsequent thermal treatment in a DSC. Further details about sample preparation for the individual analysis methods are provided below.

Instrumentation. Fast Scanning Chip Calorimetry (FSC). FSC served for subjecting PLLA to well-defined crystallization and crystal-reorganization pathways, taking advantage of the opportunities of fast cooling and heating.⁴⁴ The specimens were placed on UFS 1 chip sensors of a Flash DSC 1 from Mettler-Toledo (Greifensee, Switzerland), with the instrument connected to a TC100 intracooler (Huber, Offenburg, Germany). The sample support temperature was set to -90 °C, and the sample environment was purged with nitrogen gas at a flow rate of 35 mL/min. Besides the plain use of the FSC instrument as a sample-preparation device, heating scans on PLLA containing α' -crystals were collected to obtain their melting temperature and fine-tune the conditions of crystal reorganization, as well as to follow the α'/α -phase transformation by analysis of melting temperatures.

Differential Scanning Calorimetry (DSC). Similarly, as in the case of FSC, DSC was employed for the preparation of PLLA samples of specific crystallization routes for WAXS, SAXS, and POM analyses using a DSC 1 from Mettler-Toledo (Greifensee, Switzerland), with an attached TC100 intracooler (Huber, Offenburg, Germany). The specimens were punched from the compression-molded films and encapsulated in small 20 μL aluminum pans for thermal treatment. The furnace was purged with nitrogen gas at a flow rate of 60 mL/min. Also, heating scans were recorded to monitor changes in the structure as a result of prior thermal treatments.

Polarized-Light Optical Microscopy (POM). POM served for analysis of the micrometer-scale semicrystalline morphology of PLLA

containing α' -crystals, before and after reorganization via local and global melting. Imaging of the FSC samples was performed using an OPN 184 microscope (Kern & Sohn GmbH, Balingen, Germany), operated in the reflection mode, with images captured with a DFK 33UX252 camera (The Imaging Source Europe GmbH, Bremen, Germany). DSC samples were cut with a microtome CUT 5062 (Slee, Mainz, Germany) to obtain thin sections, which were then observed in the transmission mode between crossed polarizers in a DMRX microscope (Leica, Wetzlar, Germany) and imaged with a CCD camera (Motic, Wetzlar, Germany).

Atomic Force Microscopy (AFM). The morphology of α' - and α -crystals of PLLA and their spatial arrangement were analyzed with a Dimension FASTSCAN AFM (Bruker Corporation, Billerica, MA, USA), which was operated in the peak-force tapping mode using a peak-force set point of 20 mV. We employed Bruker silicon nitride ScanAsyst-FLUID+ sensors (Bruker Corporation, Billerica, MA, USA) with a nominal spring constant and tip radius of 0.7 N/m and 2 nm, respectively. For imaging of the surface structure of the FSC samples, the ceramic frame of the UFS 1 sensor was removed before placing the sample-loaded silicon nitride/oxide membrane onto the sample stage of the AFM, with more examples of AFM analysis of FSC samples reported elsewhere.^{45–47}

Wide- and Small-Angle X-Ray Analysis (WAXS and SAXS). WAXS and SAXS analyses were used to obtain crystal structure information and long periods of samples crystallized at different thermal pathways. Measurements were done at room temperature in the transmission mode using a Retro-F laboratory setup (SAXSLAB, Copenhagen, Denmark) operated with a microfocus X-ray source combined with an ASTIX multilayer X-ray optics (AXO Dresden GmbH, Dresden, Germany) as a monochromator, yielding $\text{CuK}\alpha$ radiation with a wavelength (λ) of 0.154 nm. The size of the double-slit generated, approximately rectangular beam was either about 0.4 (SAXS) or 0.9 mm (WAXS), and the exposure time was 300 and 600 s for WAXS and SAXS analyses of DSC samples, respectively, and 600 s for WAXS analysis of FSC samples. The intensity of scattered X-rays was recorded by a 2D PILATUS3 R 300 K detector (DECTRIS Ltd., Baden, Switzerland), and the calibration of the sample-to-detector distance was done using silver behenate as a standard. An azimuthal average of the intensity collected with the 2D detector gives the scattering signal as a function of either scattering angle 2θ or scattering vector $q = ((4\pi)/\lambda)\sin\theta$. For X-ray analysis of samples prepared in the DSC, the aluminum encapsulation was removed, while in the case of FSC samples, for easy positioning in the X-ray beam, specimens were kept on the FSC sensor.

RESULTS AND DISCUSSION

Generation of PLLA Containing α' -Crystals and Their Transformation to α -Crystals. Figure 1 provides general information about thermal pathways for the generation of PLLA containing α' -crystals [path (a)] and PLLA containing α -crystals formed by reorganization of the initial structure/ α' -crystals at elevated temperature [pathways (b1) and (b2)]. For clarity, details of the temperature–time protocols are omitted and reported on the (below) presentation of specific results. Growth of α' -crystals, in the present work, is done by isothermal annealing the melt at 90 °C (see blue segment in the left scheme), with the crystallization temperature T_c reached by direct cooling the melt from a temperature higher than $T_{m,0}$ (solid line), that is, by hot-crystallization (hc). Alternatively, the equilibrium melt was first cooled to 60 °C to permit isothermal formation of nuclei within 300 s,^{48,49} followed by reheating to T_c (dash line); the latter, cold-crystallization path (cc), due to the higher nucleation density, reduces the crystallization time and leads to a slightly finer micrometer-scale morphology without affecting the crystal morphology, as will be shown below. Heating of α' -crystals causes their melting at $T_{m,\alpha'}$ at around 150

°C,²² which is indicated with the sketched melting peak in the final heating scan of experiment (a).

The center and right thermal profiles in Figure 1 illustrate pathways of reorganization of α' - into α -crystals by global and local melting of α' -crystals, followed by melt-crystallization, respectively. The term “global melting” is used synonymously for a melting process involving complete melting of all α' -crystals to yield a fully amorphous state before fast (isothermal) recrystallization of the melt containing crystal remnants; these can be regions of lower entanglement density or of not fully relaxed chain segments, which then allow fast recrystallization.^{50,51} In this work, α' -crystals were heated to a temperature between 155 and 160 °C, that is, to a temperature slightly higher than the maximum of the FSC melting peak, and then isothermally annealed, with global melting at such condition documented in the literature.^{22,52} The growth of α -crystals is then detectable by the increased melting temperature, as indicated with the red-drawn peak in the final heating scan of the experiment (b1). Note that the conditions of global melting and melt-recrystallization were subject to slight variations in both FSC and DSC experiments to ensure optimum crystal transformation-conditions, as indicated with the red crossed arrows.

Again, the purpose of the α' - to α -crystal reorganization experiments is to change the crystal structure/density without qualitatively affecting the initial α' -crystals containing semicrystalline morphology and their effect on the presence of a long-period peak in the SAXS pattern. At this point, it may be argued that global melting and melt-recrystallization, indeed, cause a qualitative change in the semicrystalline morphology, and for this reason also, the α'/α -crystal transformation path (b2) is applied, assuming that in this case changes in the semicrystalline morphology are further minimized. The transformation path (b2) anticipates local, that is, incomplete melting of α' -crystals and recrystallization at a temperature slightly below the temperature of global melting of α' -crystals. As such, this process may also be considered as a solid–solid phase transformation, as frequently suggested in the literature.^{13,18} This transformation route is rather slow, with the needed annealing time to generate α -crystals increasing with decreasing temperature^{53,54} and with the progress of the transformation, like in the case of path (b1), assessable by analysis of the change in melting temperature. Also here, the crystal-transformation conditions were subject to slight variations to obtain information about its kinetics (see crossed red arrows). As a general comment regarding the “local” melting and crystal-reorganization path, we assume that this process may involve not only an intralamellar change of the crystal structure but also lamellar thickening, thus requiring conformational changes of molecule segments at the crystal basal planes and in crystal-near amorphous regions. PLLA, including the α' -phase, has been classified as a crystal-mobile polymer, allowing for intracrystalline chain diffusion also at temperatures below their melting temperature,^{55,56} perhaps supporting the α' - to α -crystal phase transformation.

As indicated with the square symbols, the semicrystalline morphology of PLLA containing α' -crystals on one side and PLLA containing α -crystals formed by reorganization of α' -crystals-containing PLLA on the other side is then analyzed by DSC, POM, AFM, WAXS, and SAXS.

Figure 2 shows DSC (lower part) and FSC (upper part) heating scans of PLLA of different crystallization histories for further illustration of the crystal-reorganization pathways shown

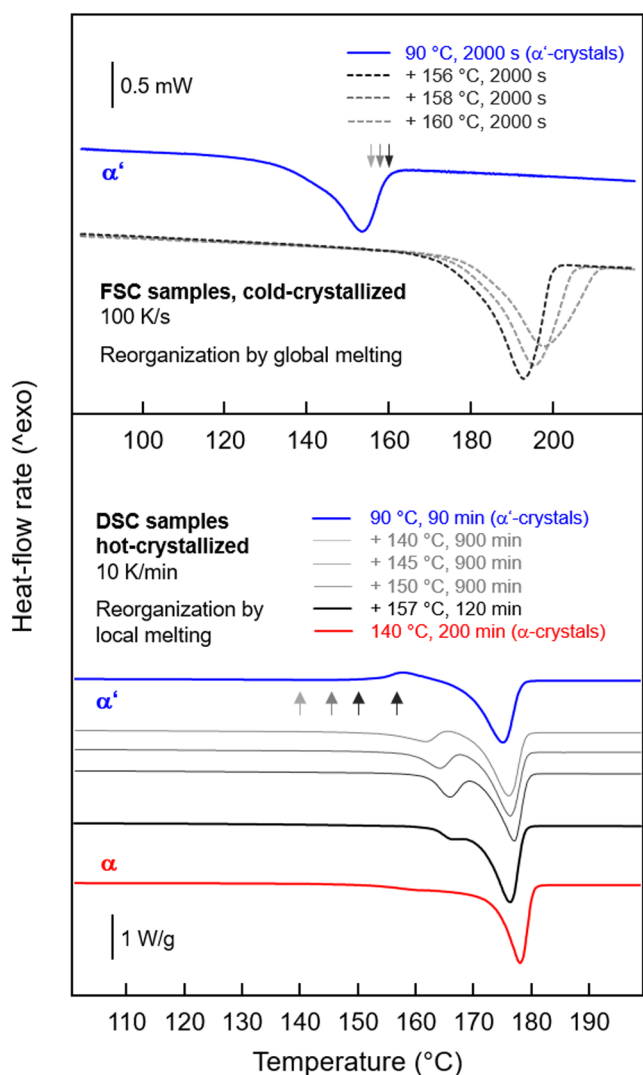


Figure 2. DSC (lower set of curves) and FSC scans (upper set of curves) of PLLA of different crystallization/reorganization histories obtained on heating at rates of 0.167 K/s (10 K/min) and 100 K/s, respectively. PLLA was crystallized at 90 °C to obtain α' -crystals, with their melting behavior on slow and fast heating represented with the blue curves, and subsequently annealed at temperatures indicated by the vertical gray/black arrows, allowing for reorganization via local (in the DSC) or global melting of α' -crystals (in the FSC). The melting of reorganized PLLA is shown with gray/black heating curves. For comparison, the lower panel of curves also includes a DSC heating scan obtained on PLLA containing α -crystals grown at 140 °C (red).

in Figure 1. Isothermal crystallization at 90 °C yields crystals with a melting temperature of around 150 °C, indicating the formation of the α' -phase (see blue curves). Heating at 100 K/s, as realized in the FSC experiment, inhibits their reorganization to α -crystals, thus allowing us to assess their stability limit. Slow heating at 10 K/min, in contrast, causes endothermic melting, which is superimposed by fast exothermic melt-recrystallization, yielding α -crystals with a higher melting temperature of close to 180 °C; further details of the melting and reorganization behaviors of α' -crystals are available in the literature.^{18,22,53,54,57–59} Importantly, it is suggested that annealing α' -crystals below their melting temperature, in particular in the temperature range between 140 and 150 °C, causes a (slow) solid–solid crystal transformation into α -crystals.⁵³ Such

annealing experiments were performed at 140, 145, and 150 °C for 900 min and 157 °C for 120 min, with these temperatures indicated with the vertical gray/black arrows at the DSC curve obtained on PLLA containing α' -crystals (blue curve). Reorganization of α' -crystals at these conditions produces crystals with a melting temperature higher than 160 °C, scaling with the annealing temperature, as shown with the gray/black DSC curves obtained after annealing (see onset of the low-temperature melting peak, which we interpret as the melting temperature of reorganized crystals; the high-temperature melting peak, again, is related to crystals reorganized during heating). However, though the increased melting temperature of the initial α' -crystals proves a change in their structure/stability, conclusions about whether a transformation to α -crystals occurred cannot be drawn, requiring X-ray analyses, as shown below.

The α' -crystal-reorganization route b1 in Figure 1 cannot be realized using a DSC since the rather low heating rate does not allow complete melting of α' -crystals. In other words, global melting-based reorganization into α -crystals is too fast to be suppressed during slow heating. As such, for global melting-based reorganization, FSC is employed, based on the knowledge of a critical heating rate of 30 K/s above which first complete melting of α' -crystals occurs and then fast self-seed-supported recrystallization, at temperatures slightly higher than the maximum of the α' -crystal melting peak. It is worth noting that the kinetics of both melting and melt-recrystallization depends on the chemical architecture (molar mass and stereoregularity) and temperature.^{22,54,60,61} As shown with the FSC heating curves in the upper part of Figure 2, annealing the melt of PLLA at temperatures a few K higher than the maximum of the α' -crystal-melting peak (see gray/black arrows) yields crystals that melt between 180 and 200 °C (see gray/black dashed curves), suggesting the formation of α -crystals by comparison with the melting peak of PLLA melt-crystallized at 140 °C and containing α -crystals (see red curve in the lower panel of Figure 2).

Final conclusions about the change of the crystal structure by various thermal treatments are based on the WAXS data presented in Figures 3 and 4 for DSC and FSC samples, respectively. In Figures 3 and 4, the lower panel provides an overview of collected data in a wider scattering-angle range, while the upper plot serves as a detailed illustration of the position of the intense 110/200 peak, indicative of the degree of disorder of crystals. As in Figure 2, blue and red coloring are applied to samples containing α' - and α -crystals obtained by crystallization at 90 and 140 °C, respectively, while gray/black coloring denotes that α' -crystals were subjected to an annealing/reorganization step.

The data shown in Figure 3 reveal the presence of α' - and α -crystals after hot-crystallization of PLLA at 90 and 140 °C, respectively, by both the different number and position of diffraction peaks.^{14,15,28,40,56} Conformational disorder in α' -crystals causes an enlargement of the basal plane of the unit cell, with the intense 110/200 peak therefore being located at a lower scattering angle than in the case of α -crystals (see upper panel of Figure 3). In addition, due to the higher perfection of α -crystals, additional peaks are detected, with some of them marked by red arrows.⁶² Reorganization of α' -crystals by local melting and recrystallization causes not only a reduction of disorder, as is best seen by the shift of the strong 110/200 peak to a higher scattering angle, but also the appearance of additional peaks. In addition, it is also observed that the degree of reorganization of

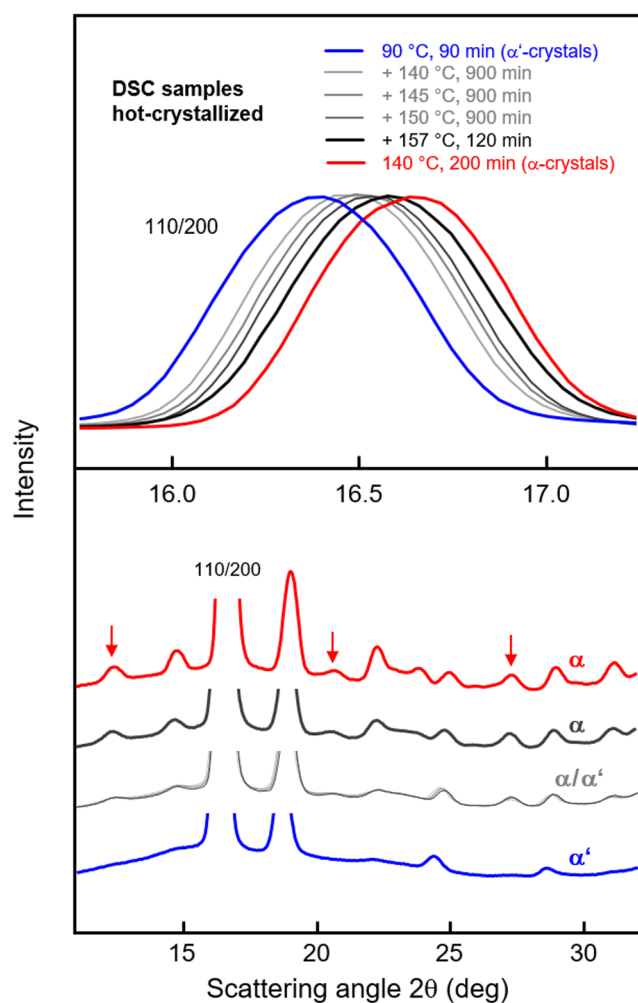


Figure 3. WAXS curves of PLLA of different crystallization and reorganization histories, as indicated in the legend, prepared in a DSC. The lower panel shows the WAXS curves in a wider scattering-angle range, while the upper plot is an enlargement showing the most intense 110/200 peak. For improved comparison of peak positions, curves were manually scaled regarding their intensity, to account for different absorption/scattering intensities when analyzing samples of slightly different thickness. The coloring of curves is analogous to the data presented in Figure 2. The red arrows in the lower panel indicate PLLA peaks, which are only observed when α -crystals are present. Complete indexing of scattering peaks is omitted since it is not required within the scope of this study and, in part, is not consistent in the literature.^{12,13,17,62}

α' -crystals toward the structure of α -crystals increases with the annealing temperature from 140 to 157 °C, but without achieving a structural state/perfection as after hot-crystallization of the quiescent melt at 140 °C. The observation of incomplete reorganization is also in strong agreement with the analysis of melting temperatures, presented in Figure 2. At best, annealing at 157 °C for 2 h may have produced α -crystals. It is worth noting that the perfection of crystals by annealing at a specific temperature also increases with the annealing time, which, however, is not evaluated further here.

Though out of focus of the present work, visual inspection of the shape and half-width of the 110/200 peak of PLLA of different crystallization and reorganization histories suggests the presence of a single crystal population in reorganized samples. In other words, crystals of PLLA can exhibit a large variety of

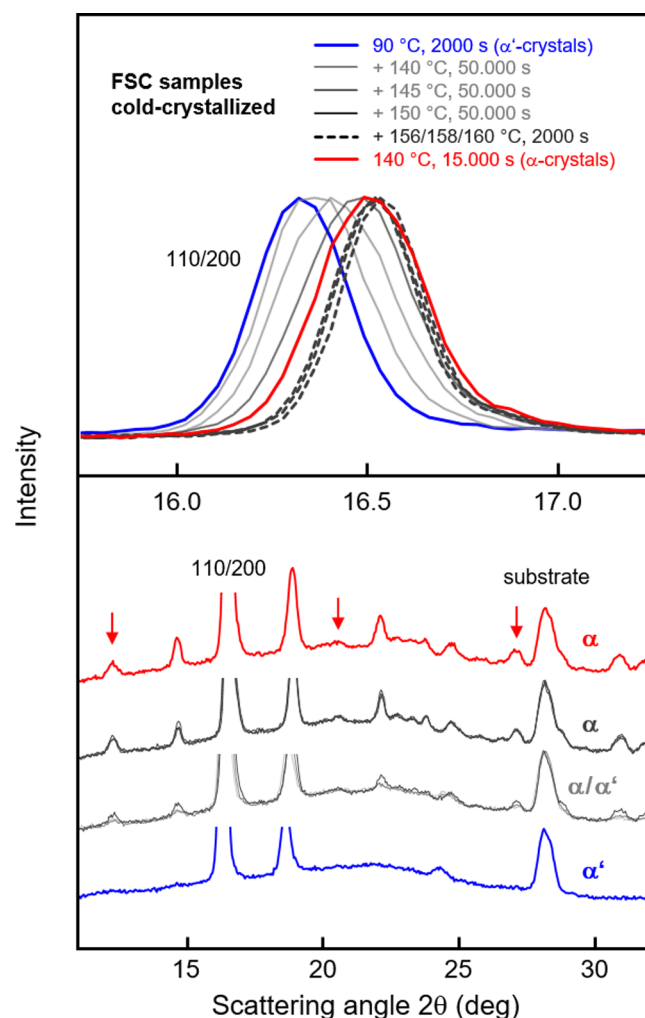


Figure 4. WAXS curves of PLLA of different crystallization and reorganization histories, as indicated in the legend, prepared in an FSC. The lower panel shows the WAXS curves in a wider scattering-angle range, while the upper plot is an enlargement showing the most intense 110/200 peak. For improved comparison of peak positions, curves were manually scaled regarding their intensity to account for different absorption/scattering intensities when analyzing samples of slightly different size. The coloring of curves is in analogy to the data presented in Figure 2. The FSC samples were not detached from the silicon nitride/oxide membrane of the sensor, and therefore, the shown WAXS curves include a halo-like scattering component and an additional peak labeled “substrate.” The red arrows in the lower panel indicate PLLA peaks, which are only observed when α -crystals are present. Complete indexing of scattering peaks is omitted since it is not required within the scope of this study and, in part, is not consistent in the literature.^{12,13,17,62}

disorder, and the often described polymorphism is not limited to the formation of α' - and α -crystals only. It may be speculated whether melt-crystallization between 100 and 120 °C leads – as often suggested based on analysis of the 203 scattering peak – to simultaneous formation of α' - and α -crystals^{13,63} or to crystals with a degree of disorder in between α' - and α -crystals.¹⁸ An analysis of the melting behavior by FSC, suppressing reorganization on heating, may provide final evidence for either interpretation.

The WAXS data shown in Figure 4, obtained on FSC samples, confirm the results obtained on DSC samples. Crystallization at 90 and 140 °C yields α' - and α -crystals, respectively, and

reorganization by local melting at temperatures lower than the stability limit of α' -crystals, between 140 and 150 °C, at least within the frame of the selected annealing time of 50,000 s, improves the crystal perfection without reaching the structure of PLLA melt-crystallized at 140 °C (see gray curves). Reorganization at temperatures between 156 and 160 °C, with the annealing temperature reached by fast heating at 100 K/s (which is higher than the critical heating rate to suppress solid-state reorganization), proceeding via global melting and melt-recrystallization, generates α -crystals, as shown with the black/dashed curves. Obviously, as long as complete melting of α' -crystals in the reorganization experiment is allowed, an effect of the reorganization temperature on the structure of regrown crystals, at least within the selected limits, is not observed.

The data obtained on FSC samples/ α' -crystals reorganized via global melting are in agreement with the X-ray data (see dashed curves in the upper panel of Figure 2), as the melting temperature is well above 180 °C. The increase in melting temperature indicates the growth of larger crystals if the reorganization temperature increases, without a measurable change in the unit cell.

Micrometer-Scale Semicrystalline Morphology of PLLA Containing α' -Crystals, Before and After Reorganization via Local and Global Melting. Figure 5 shows POM images of PLLA subjected to different crystallization–reorganization pathways, obtained on FSC (left column) and DSC samples (right column). As before (see Figures 2–4), the initial melt-crystallization step at 90 °C to obtain α' -crystals was done by cold- and hot-crystallization in the case of FSC and DSC samples, respectively, with their superstructures shown with the top images. Cold-crystallization results in a distinctly finer morphology than hot-crystallization, due to the higher number of crystal nuclei generated at the nucleation temperature of 60 °C within 5 min, without the possibility to recognize the location of former nuclei. In the case of hot-crystallization, in contrast, the nuclei number is much lower, allowing the growth of rather large spherulites with a diameter of around 20 μm .

Most important, as shown with the center- and bottom-row images, is the observation of an unchanged semicrystalline morphology after isothermal reorganization below and above the maximum stability limit of the α' -crystals, with the latter, again, defined by the FSC melting peak detected on heating at 100 K/s (see blue curve in the upper panel of Figure 2). As such, the POM images obtained on reorganized PLLA support the experimental idea of evaluating the effect of the crystal density on the detection of long-periodicity by SAXS, without an overall change in the crystalline–amorphous superstructure.

Briefly continuing/confirming the discussion of the effect of heating rate on allowing reorganization of α' -crystals via global melting, the POM image of the DSC sample, which was crystallized at 90 °C and then slowly heated at 10 K/min to the reorganization temperature of 157 °C (bottom right image), that is, to a temperature higher than the FSC melting peak obtained on fast heating, reveals the absence of global melting, as in such case, a significantly finer structure would have been expected. Typically, melt-recrystallization via self-nucleation is based on remnants (nonisotropic amorphous domains) of former crystals, with their number being much higher than the number of spherulites present in the initial sample.^{51,64,65} As such, reorganization of PLLA containing α' -crystals via global melting only is possible by FSC when approaching the reorganization temperature at sufficiently high rate.

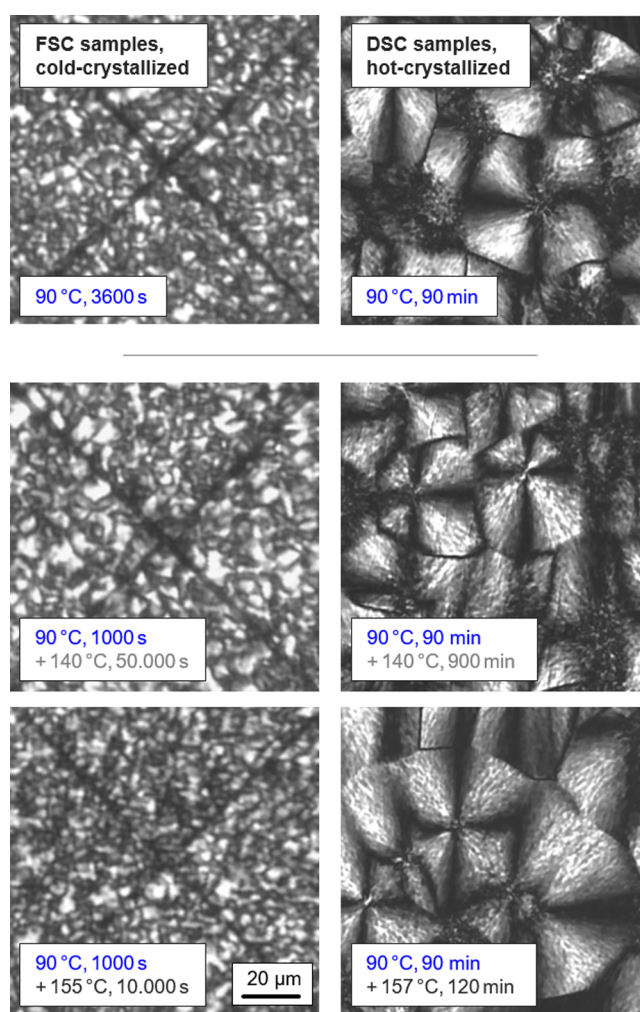


Figure 5. POM images of PLLA of different crystallization histories, as indicated in the legends. The samples were prepared either by cold-crystallization in an FSC, with the visible, crossing diagonals originating from the FSC sensor membrane (left-column images) or by hot-crystallization in a DSC (right-column images). The scale bar holds for all images, and the polarizer directions are parallel to the image borders.

Nanometer-Scale Semicrystalline Morphology of PLLA Containing α' -Crystals, Before and After Reorganization via Local and Global Melting.

A key issue in the context of interpretation of the absence a long-period maximum in the SAXS pattern of PLLA containing α' -crystals, frequently reported in the literature,^{29–33} is gaining ultimate knowledge about the nanometer-scale morphology, that is, the habit and arrangement of crystals, by direct imaging. As such, Figure 6 displays AFM images of the surface structure of FSC samples of PLLA crystallized at 90 °C, thus containing α' -crystals. To increase confidence in the observed results, imaging was done using samples of different sources, which, in addition, were subjected to different nucleation routes. In detail, the top left image was obtained by cold-crystallization (cc); otherwise, the hot-crystallization (hc) route was applied (see cc- and hc-pathways in the left scheme of Figure 1). Furthermore, the top and bottom two images were collected on PLLA provided by Corbion and Sulzer, respectively.

All images, regardless of the specific PLLA grade and the nucleation pathway, provide consistent information about the semicrystalline morphology of PLLA containing α' -crystals at

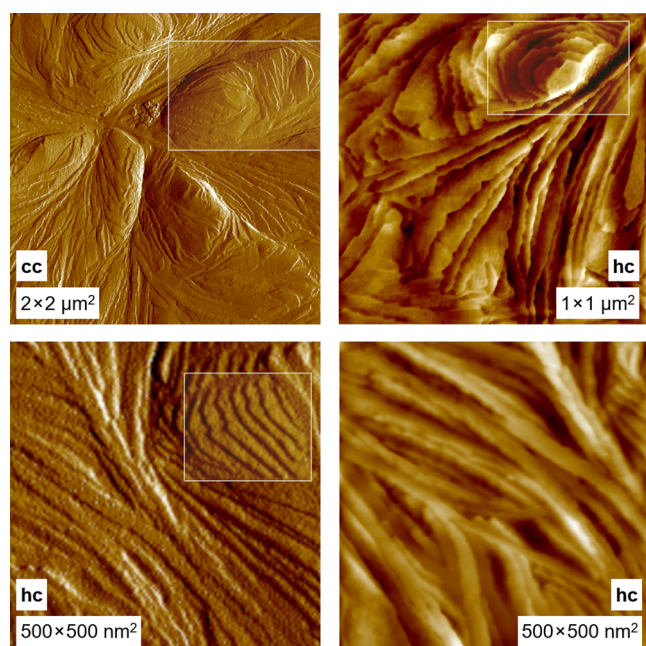


Figure 6. AFM images of PLLA crystallized at 90 °C in an FSC, containing α' -crystals. The images were obtained on PLLA of different sources, Corbion- (top) and Sulzer-grade PLLA (bottom), and on samples either cold- or hot-crystallized, as indicated in the images with the labels “cc” and “hc,” respectively. The framed areas emphasize the presence of terrace-like stacked lamellae. The figure contains both height and error images, which were selected for optimum presentation of structural features.

the nanometer scale. As such, α' -crystals are of lamellar shape, with the lamellae forming stacks in the direction of their short dimension, as advantageously illustrated with flat-on or nearly flat-on viewed terrace-like structures (see framed areas). Though AFM, in this study, is not used to obtain quantitative information about the thickness of lamellae, to avoid errors due to tip-smearing,^{66,67} or tilt of lamellae, visual inspection of the images suggests that the lateral dimension of the lamellae is of the order of magnitude of several hundreds of nanometers, and that lamellar stacks may contain more than 10 lamellae. It is worth mentioning that, as emphasized with the framed area in the top left image of cold-crystallized PLLA, the lamellar stacks may be considered as semicrystalline clusters with a lateral size of around 1 μm , similar to what was observed for the heterogeneities detected by POM (see top left image in Figure 5).

Figure 7 shows AFM images of PLLA initially crystallized at 90 °C to obtain α' -crystals and thermally treated to permit their global (top images) or local melting (bottom images), followed by isothermal recrystallization. As seen in Figure 6, the left and right images were collected on PLLA of different sources, with the initial structure developed during hot- and cold-crystallization, respectively, as indicated. Global melting and melt-recrystallization yield laterally extended lamellae, similar to that in the initial structure (see Figure 6) which, however, appear thicker, likely caused by the high recrystallization temperature of 156 °C (left image) or 155 °C (right image).⁶⁸ Note that an in-depth discussion of the effect of the crystallization temperature (90 °C versus 155 or 156 °C) on the lamellar thickness is out of the scope here, as it would require knowledge of the supercooling of the melt during crystallization and, with that, of the equilibrium melting temperature of the different crystal

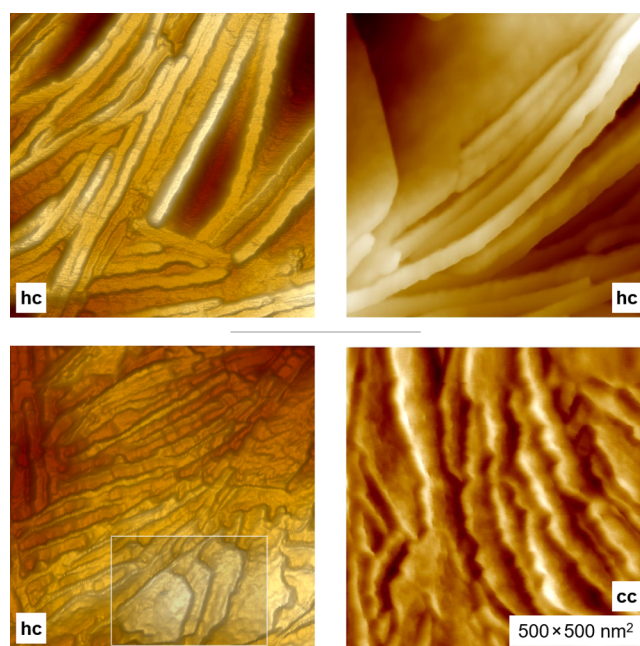


Figure 7. AFM images of PLLA subjected to the formation of α' -crystals at 90 °C in an FSC via hot- or cold-crystallization, as indicated with the labels “cc” and “hc,” respectively, followed by recrystallization via global (top images) or local melting (bottom images). The left and right images were obtained on Sulzer- and Corbion-grade PLLA, respectively. The scanned area of 500 nm² is identical for all images, and the framed area in the bottom left image, as in Figure 6, emphasizes the presence of nearly flat-on viewed lamellae/lamellar stacks. The figure contains both height and error images, which were selected for optimum presentation of structural features.

polymorphs, not known for α' -crystals. Also, for PLLA reorganized (or partly reorganized) via a quasi solid–solid transformation of the crystal structure at 140 °C, preservation of the initial lamellar morphology formed at 90 °C is detected, but with the lamellae appearing thinner than after global melting and recrystallization at around 155 °C and with the visible (growth-)surfaces appearing rough or nonflat. Careful inspection of the AFM image of nonreorganized PLLA (see top right image in Figure 6), however, yielded a similar feature, which therefore may not necessarily be caused by the annealing process at 140 °C.

The experimental results discussed in Figures 2–7 confirm the presence of different crystal structures (α' - and α -crystals) in PLLA of qualitatively similar semicrystalline morphology, achieved by specific crystal reorganization routes without destroying the memory of the initial melt-crystallization. The latter is, in particular, demonstrated with the preserved micrometer- and nanometer-scale structures shown in Figures 5–7. All samples, regardless of the prevailing crystal polymorph, contain lamellar crystals that are arranged within stacks, suggesting long-distance periodicity. These samples are analyzed in the following sections regarding their SAXS pattern, to yield conclusion about the detection of long-period peaks.

SAXS of PLLA Containing Either α' - or α -Crystals within Qualitatively Similar Semicrystalline Environments. Figure 8 shows SAXS data of PLLA crystallized at 90 °C (blue curves) and subsequently isothermally reorganized (gray and black curves) in an FSC (top set of curves) or DSC (bottom set of curves). The specific crystallization and reorganization conditions are provided in the legends. In

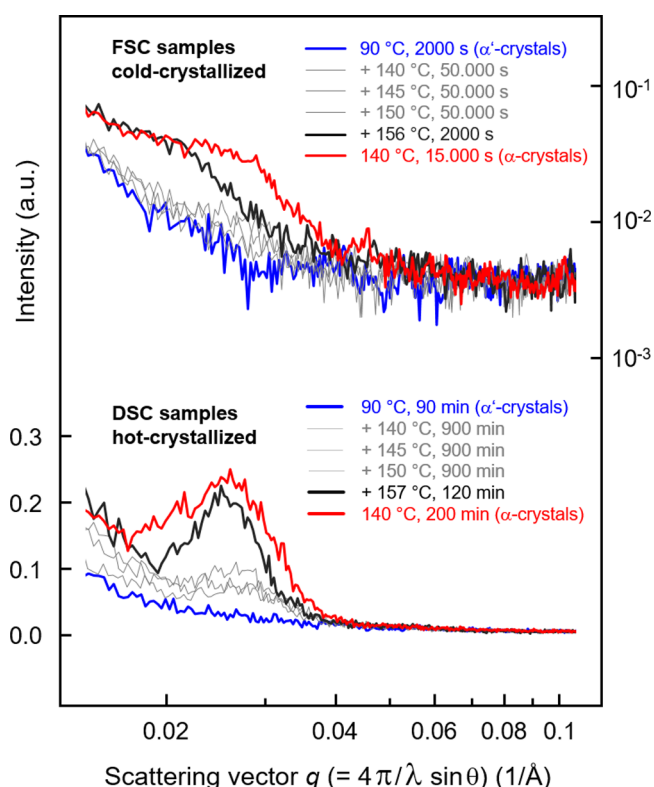


Figure 8. SAXS data of PLLA crystallized at 90 °C (blue curves) and subsequently isothermally reorganized (gray and black curves) in an FSC (top set of curves) or DSC (bottom set of curves), with the specific crystallization/reorganization conditions provided in the legends. For comparison, SAXS curves of PLLA hot-crystallized at 140 °C in the DSC and cold-crystallized at the same temperature in the FSC, both containing α -crystals, are included (red curves). The initial preparation of α' -crystals was performed by hot-crystallization (DSC samples) or cold-crystallization (FSC samples). Note that linear and logarithmic scaling of the intensity serves as an optimum visualization of the long-period peaks.

addition, for comparison, SAXS curves of PLLA hot- and cold-crystallized at 140 °C in the DSC or FSC, respectively, both containing α -crystals, are included (red curves). Initial preparation of α' -crystals was performed by hot-crystallization (DSC samples) or cold-crystallization (FSC samples). First of all, SAXS curves obtained on DSC and FSC samples suggest similar trends regarding the observation of a long-period peak as a function of the crystallization/reorganization conditions, despite the rather large noise/scatter of data collected from the small FSC samples with a mass of only a few hundred nanograms.

In both cases, after hot- and cold-crystallization at 90 °C in the DSC and FSC, respectively, connected with the growth of α' -crystals, a long-period peak cannot be detected in the SAXS patterns (see blue curves), though AFM images provide evidence of the presence of lamellar crystals and their stacking in the direction of the fold surface (Figure 6). Note that also long-term annealing of PLLA at the crystallization temperature of 90 °C, involving secondary crystallization,^{23,25} does not lead to a change of the SAXS curve.

Partial reorganization of α' - into α -crystals by local melting and recrystallization (see path b2 in Figure 1, and the corresponding WAXS patterns in Figures 3 and 4, gray curves) causes the appearance of a small SAXS peak. Quantitative

evaluation of data obtained on DSC samples (evaluation of SAXS curves collected from FSC samples was omitted due to their large noise) suggests a long period of around 22 nm. Reorganization of PLLA containing α' -crystals at a temperature higher than 155 °C, involving at least for the FSC sample global melting, produces an even larger long-period peak (black curves), paralleled by the formation of α -crystals (see corresponding WAXS data in Figures 3 and 4). The position of the SAXS peak (of the DSC sample) shifted to a slightly lower value of the scattering vector q , indicating a minor increase in the long period to almost 25 nm, being slightly higher than the value observed after crystallization of the isotropic melt at 140 °C (see red curves), being 24 nm.

The evolution of a distinct long-period peak after thermal treatment of PLLA initially containing α' -crystals is clearly caused by an overall increase in the intensity of the SAXS signal. Such an effect is to be expected, as the SAXS signal of a two-phase system (here crystalline and amorphous regions) is proportional to the square of the density difference between the crystalline and amorphous phases, $I \approx (\rho_{\text{cry}} - \rho_{\text{am}})^2$.⁶⁹ It means that the density of α' -crystals is so close to the density of the amorphous regions that the scattering signal is too weak to be observable, while the transition to the α -phase, with its larger density, causes an increase in the scattering intensity.

CONCLUSIONS

Crystallization of poly(L-lactic acid) (PLLA) at 90 °C leads to the formation of disordered α' -crystals of lamellar shape. These lamellae form stacks, however, with a long period not detectable by SAXS. The main reason is the low density contrast between the amorphous phase and the crystal lamellae. This conclusion is based on detailed AFM imaging of the α' -phase, and specific crystal-reorganization experiments, in which the lower-density disordered α' -crystals are transformed, either completely or only partially, into higher-density α -crystals, without large-scale reorganization of the semicrystalline morphology/spatial rearrangement of the amorphous and crystalline phases, leading to the appearance of SAXS peaks with an intensity that scales with the degree of the phase transformation/change of the crystal density.

AUTHOR INFORMATION

Corresponding Author

René Androsch – Interdisciplinary Center for Transfer-Oriented Research in Natural Sciences (IWE TFN), Martin Luther University Halle-Wittenberg, Halle/Saale 06099, Germany; orcid.org/0000-0002-7924-0159; Email: rene.androsch@iw.uni-halle.de

Authors

Katalee Jariyavidyanont – Interdisciplinary Center for Transfer-Oriented Research in Natural Sciences (IWE TFN), Martin Luther University Halle-Wittenberg, Halle/Saale 06099, Germany; orcid.org/0000-0001-8240-126X

Andreas Janke – Leibniz-Institut für Polymerforschung Dresden e.V., Dresden 01069, Germany

Qiang Yu – Institute of Physics, Martin Luther University Halle-Wittenberg, Halle/Saale 06099, Germany

Thomas Thurn-Albrecht – Institute of Physics, Martin Luther University Halle-Wittenberg, Halle/Saale 06099, Germany; orcid.org/0000-0002-7618-0218

Complete contact information is available at: <https://pubs.acs.org/10.1021/acs.cgd.3c01498>

Author Contributions

The manuscript was written through the contributions of all authors, and all authors have given approval to the final version of the manuscript.

Notes

The authors declare no competing financial interest.

ACKNOWLEDGMENTS

Q.Y. and T.T.A. acknowledge funding by the Deutsche Forschungsgemeinschaft (DFG, German Research Foundation) – Project-ID 189853844 – TRR 102.

REFERENCES

- (1) Garlotta, D. A literature review of poly (lactic acid). *J. Polym. Env.* **2001**, *9*, 63–84.
- (2) Pang, X.; Zhuang, X.; Tang, Z.; Chen, X. Polylactic acid (PLA): Research, development and industrialization. *Biotechn. J.* **2010**, *5*, 1125–1136.
- (3) Nampoothiri, K. M.; Nair, N. R.; John, R. P. An overview of the recent developments in polylactide (PLA) research. *Bioresour. Technol.* **2010**, *101*, 8493–8501.
- (4) Nguyen, H. T. H.; Qi, P.; Rostagno, M.; Feteha, A.; Miller, S. A. The quest for high glass transition temperature bioplastics. *J. Mater. Chem. A* **2018**, *6*, 9298–9331.
- (5) Tábi, T.; Hajba, S.; Kovács, J. G. Effect of crystalline forms (α' and α) of poly (lactic acid) on its mechanical, thermo-mechanical, heat deflection temperature and creep properties. *Eur. Polym. J.* **2016**, *82*, 232–243.
- (6) Pyda, M.; Bopp, R. C.; Wunderlich, B. Heat capacity of poly (lactic acid). *J. Chem. Therm.* **2004**, *36*, 731–742.
- (7) Zhang, R.; Du, F.; Jariyavidyanont, K.; Zhuravlev, E.; Schick, C.; Androsch, R. Glass transition temperature of poly (D, L-lactic acid) of different molar mass. *Thermochim. Acta* **2022**, *718*, 179387.
- (8) Salmerón Sánchez, M.; Mathot, V. B. F.; Vanden Poel, G.; Gómez Ribelles, J. L. Effect of the cooling rate on the nucleation kinetics of poly (L-lactic acid) and its influence on morphology. *Macromolecules* **2007**, *40*, 7989–7997.
- (9) De Santis, F.; Pantani, R.; Titomanlio, G. Nucleation and crystallization kinetics of poly (lactic acid). *Thermochim. Acta* **2011**, *522*, 128–134.
- (10) Androsch, R.; Iqbal, H. M. N.; Schick, C. Non-isothermal crystal nucleation of poly (L-lactic acid). *Polymer* **2015**, *81*, 151–158.
- (11) Zhang, J.; Duan, Y.; Sato, H.; Tsuji, H.; Noda, I.; Yan, S.; Ozaki, Y. Crystal modifications and thermal behavior of poly (L-lactic acid) revealed by infrared spectroscopy. *Macromolecules* **2005**, *38*, 8012–8021.
- (12) Pan, P.; Kai, W.; Zhu, B.; Dong, T.; Inoue, Y. Polymorphous crystallization and multiple melting behavior of poly (L-lactide): Molecular weight dependence. *Macromolecules* **2007**, *40*, 6898–6905.
- (13) Zhang, J.; Tashiro, K.; Tsuji, H.; Domb, A. J. Disorder-to-order phase transition and multiple melting behavior of poly (L-lactide) investigated by simultaneous measurements of WAXD and DSC. *Macromolecules* **2008**, *41*, 1352–1357.
- (14) De Santis, P.; Kovacs, A. Molecular conformation of poly (S-lactic acid). *Biopolymers* **1968**, *6* (3), 299–306.
- (15) Wasanasuk, K.; Tashiro, K.; Hanesaka, M.; Ohhara, T.; Kurihara, K.; Kuroki, R.; Tamada, T.; Ozeki, T.; Kanamoto, T. Crystal structure analysis of poly (L-lactic acid) α form on the basis of the 2-dimensional wide-angle synchrotron X-ray and neutron diffraction measurements. *Macromolecules* **2011**, *44*, 6441–6452.
- (16) Lotz, B. Crystal polymorphism and morphology of polylactides. *Adv. Polym. Sci.* **2017**, *279*, 273–302.
- (17) Wasanasuk, K.; Tashiro, K. Crystal structure and disorder in poly (L-lactic acid) δ form (α' form) and the phase transition mechanism to the ordered α form. *Polymer* **2011**, *52*, 6097–6109.
- (18) Kawai, T.; Rahman, N.; Matsuba, G.; Nishida, K.; Kanaya, T.; Nakano, M.; Okamoto, H.; Kawada, J.; Usuki, A.; Honma, N.; Nakajima, K.; Matsuda, M. Crystallization and melting behavior of poly (L-lactic acid). *Macromolecules* **2007**, *40*, 9463–9469.
- (19) Kalish, J. P.; Aou, K.; Yang, X.; Hsu, S. L. Spectroscopic and thermal analyses of α' and α crystalline forms of poly (L-lactic acid). *Polymer* **2011**, *52*, 814–821.
- (20) Zhang, J.; Tashiro, K.; Domb, A. J.; Tsuji, H. Confirmation of disorder α form of poly (L-lactic acid) by the X-ray fiber pattern and polarized IR/Raman spectra measured for uniaxially-oriented samples. *Macromol. Symp.* **2006**, *242*, 274–278.
- (21) Di Lorenzo, M. L.; Cocca, M.; Malinconico, M. Crystal polymorphism of poly (L-lactic acid) and its influence on thermal properties. *Thermochim. Acta* **2011**, *522*, 110–117.
- (22) Androsch, R.; Schick, C.; Di Lorenzo, M. L. Melting of conformationally disordered crystals (α' -phase) of poly (L-lactic acid). *Macromol. Chem. Phys.* **2014**, *215*, 1134–1139.
- (23) Jariyavidyanont, K.; Schick, C.; Androsch, R. The bulk enthalpy of melting of α' -crystals of poly (L-lactic acid) determined by fast scanning chip calorimetry. *Thermochim. Acta* **2022**, *717*, 179349.
- (24) Di Lorenzo, M. L.; Androsch, R. Influence of α' -/ α -crystal polymorphism on properties of poly (L-lactic acid). *Polym. Int.* **2019**, *68*, 320–334.
- (25) Jariyavidyanont, K.; Yu, Q.; Petzold, A.; Thurn-Albrecht, T.; Glüge, R.; Altenbach, H.; Androsch, R. Young's modulus of the different crystalline phases of poly (L-lactic acid). *J. Mech. Beh. Biomed. Mater.* **2023**, *137*, 105546.
- (26) Yasuniwa, M.; Tsubakihara, S.; Iura, K.; Ono, Y.; Dan, Y.; Takahashi, K. Crystallization behavior of poly (L-lactic acid). *Polymer* **2006**, *47*, 7554–7563.
- (27) Abe, H.; Kikkawa, Y.; Inoue, Y.; Doi, Y. Morphological and kinetic analyses of regime transition for poly [(S)-lactide] crystal growth. *Biomacromolecules* **2001**, *2*, 1007–1014.
- (28) Kanchanasopa, M.; Manias, E.; Runt, J. Solid-state microstructure of poly (L-lactide) and L-lactide/meso-lactide random copolymers by atomic force microscopy (AFM). *Biomacromolecules* **2003**, *4*, 1203–1213.
- (29) Huang, J.; Lisowski, M. S.; Runt, J.; Hall, E. S.; Kean, R. T.; Buehler, N.; Lin, J. S. Crystallization and microstructure of poly (L-lactide-co-meso-lactide) copolymers. *Macromolecules* **1998**, *31*, 2593–2599.
- (30) Baratian, S.; Hall, E. S.; Lin, J. S.; Xu, R.; Runt, J. Crystallization and solid-state structure of random polylactide copolymers: Poly (L-lactide-co-D-lactide)s. *Macromolecules* **2001**, *34*, 4857–4864.
- (31) Cho, J.; Baratian, S.; Kim, J.; Yeh, F.; Hsiao, B. S.; Runt, J. Crystallization and structure formation of poly (L-lactide-co-meso-lactide) random copolymers: A time-resolved wide-angle X-ray scattering study. *Polymer* **2003**, *44*, 711–717.
- (32) Díez-Rodríguez, T. M.; Blázquez-Blázquez, E.; Martínez, J. C.; Cerrada, M. L.; Pérez, E. A synchrotron SAXS study of PLLA crystallized at different temperatures: One-dimensional correlation functions. *Polymer* **2022**, *256*, 125232.
- (33) Cho, T. Y.; Strobl, G. Temperature dependent variations in the lamellar structure of poly (L-lactide). *Polymer* **2006**, *47*, 1036–1043.
- (34) Crist, B. Analysis of small-angle X-ray scattering patterns. *J. Macromol. Sci. Part B* **2000**, *39*, 493–518.
- (35) Toda, A. Small angle X-ray scattering from finite sequence of lamellar stacks of crystalline polymers. *Polymer* **2020**, *211*, 123110.
- (36) Delpouve, N.; Saiter, A.; Mano, J. F.; Dargent, E. Cooperative rearranging region size in semi-crystalline poly (L-lactic acid). *Polymer* **2008**, *49*, 3130–3135.
- (37) Hu, J.; Wang, J.; Gowd, E. B.; Yuan, Y.; Zhang, T.; Duan, Y.; Hu, W.; Zhang, J. Small-angle and wide-angle X-ray scattering study on α' -to- α transition of poly (L-lactide acid) crystals. *Polymer* **2019**, *167*, 122–129.
- (38) Miyata, T.; Masuko, T. Morphology of poly (L-lactide) solution-grown crystals. *Polymer* **1997**, *38*, 4003–4009.
- (39) Fischer, E. W.; Sterzel, H. J.; Wegner, G. Investigation of the structure of solution grown crystals of lactide copolymers by means of chemical reactions. *Kolloid Z. Z. Polym.* **1973**, *251*, 980–990.

- (40) Wasanasuk, K.; Tashiro, K. Theoretical and experimental evaluation of crystallite moduli of various crystalline forms of poly (L-lactic acid). *Macromolecules* **2012**, *45*, 7019–7026.
- (41) Androsch, R.; Iqbal, N.; Schick, C. Non-isothermal crystal nucleation of poly (L-lactic acid). *Polymer* **2015**, *81*, 151–158.
- (42) www.sulzer.com/-/media/files/products/polymer_production_technology/brochures/fact_sheet_poly lactides.pdf (accessed 29/06/2023).
- (43) Corbion, Personal information, 10/08/2018; Total-Corbion, Product data sheet, www.totalenergies-corbion.com/media/dtnoqkxb/pds-luminy-l175-20220722.pdf (accessed 18/06/2023).
- (44) Mathot, V.; Pyda, M.; Pijpers, T.; Poel, G. V.; Van de Kerkhof, E.; Van Herwaarden, S.; Van Herwaarden, F.; Leenaers, A. The Flash DSC 1, a power compensation twin-type, chip-based fast scanning calorimeter (FSC): First findings on polymers. *Thermochim. Acta* **2011**, *522* (1–2), 36–45.
- (45) Jariyavidyanont, K.; Janke, A.; Androsch, R. Crystal self-nucleation in polyamide 11 of different semicrystalline morphology. *Polymer* **2019**, *184*, 121864.
- (46) Baeten, D.; Cavallo, D.; Portale, G.; Androsch, R.; Mathot, V.; Goderis, B. Combining fast scanning chip calorimetry with structural and morphological characterization techniques. In *Fast Scanning Calorimetry*, Schick, C.; Mathot, V., Eds.; Springer, 2016; pp. 327359.
- (47) Jariyavidyanont, K.; Zhang, R.; Yu, Q.; Janke, A.; Thurn-Albrecht, T.; Schick, C.; Androsch, R. Formation of imperfect crystals in poly (ϵ -caprolactone) at high melt-supercooling. *Mater. Lett.* **2022**, *324*, 132704.
- (48) Androsch, R.; Di Lorenzo, M. L. Crystal nucleation in glassy poly (L-lactic acid). *Macromolecules* **2013**, *46*, 6048–6056.
- (49) Androsch, R.; Di Lorenzo, M. L. Kinetics of crystal nucleation of poly (L-lactic acid). *Polymer* **2013**, *54*, 6882–6885.
- (50) Wunderlich, B. *Macromolecular Physics, Vol 2, Crystal nucleation, growth, annealing*; Academic Press: New York, 1976.
- (51) Sangroniz, L.; Cavallo, D.; Müller, A. J. Self-nucleation effects on polymer crystallization. *Macromolecules* **2020**, *53*, 4581–4604.
- (52) Androsch, R.; Zhang, R.; Schick, C. Melt-recrystallization of poly (L-lactic acid) initially containing α' -crystals. *Polymer* **2019**, *176*, 227–235.
- (53) Pan, P.; Zhu, B.; Kai, W.; Dong, T.; Inoue, Y. Polymorphic transition in disordered poly (L-lactide) crystals induced by annealing at elevated temperatures. *Macromolecules* **2008**, *41*, 4296–4304.
- (54) Androsch, R.; Zhuravlev, E.; Schick, C. Solid-state reorganization, melting and melt-recrystallization of conformationally disordered crystals (α' -phase) of poly (L-lactic acid). *Polymer* **2014**, *55*, 4932–4941.
- (55) Chen, W.; Zhou, W.; Makita, Y.; Wang, S.; Yuan, S.; Konishi, T.; Miyoshi, T. Characterization of the slow molecular dynamics of poly (L-lactic acid) in α and α' phases, in a glassy state, and in a complex with poly (D-lactic acid) by solid-state NMR. *Macromol. Chem. Phys.* **2018**, *219*, 1700451.
- (56) Schulz, M.; Schäfer, M.; Saalwächter, K.; Thurn-Albrecht, T. Competition between crystal growth and intracrystalline chain diffusion determines the lamellar thickness in semicrystalline polymers. *Nat. Commun.* **2022**, *13* (1), 119.
- (57) Ling, X.; Spruiell, J. E. Analysis of the complex thermal behavior of poly (L-lactic acid) film. I. Samples crystallized from the glassy state. *J. Polym. Sci. Polym. Phys.* **2006**, *44*, 3200–3214.
- (58) Yasuniwa, M.; Iura, K.; Dan, Y. Melting behavior of poly (L-lactic acid): Effects of crystallization temperature and time. *Polymer* **2007**, *48*, 5398–5407.
- (59) Zhu, R.; Zheng, R.; Fu, L.; Li, Z.; Yan, C. Thermal stability of poly (L-lactide) α' crystals and its blocking effect on perfection of α crystals. *Mater. Today Commun.* **2020**, *23*, 100900.
- (60) Di Lorenzo, M. L.; Androsch, R. Stability and reorganization of α' -crystals in random L/D-lactide copolymers. *Macromol. Chem. Phys.* **2016**, *217*, 1534–1538.
- (61) Androsch, R.; Di Lorenzo, M. L. Effect of molar mass on the α' / α -transition in poly (L-lactic acid). *Polymer* **2017**, *114*, 144–148.
- (62) Righetti, M. C.; Gazzano, M.; Di Lorenzo, M. L.; Androsch, R. Enthalpy of melting of α' - and α -crystals of poly (L-lactic acid). *Eur. Polym. J.* **2015**, *70*, 215–220.
- (63) Cocca, M.; Di Lorenzo, M. L.; Malinconico, M.; Frezza, V. Influence of crystal polymorphism on mechanical and barrier properties of poly (L-lactic acid). *Eur. Polym. J.* **2011**, *47* (5), 1073–1080.
- (64) Fillon, B.; Wittmann, J. C.; Lotz, B.; Thierry, A. Self-nucleation and recrystallization of isotactic polypropylene (α phase) investigated by differential scanning calorimetry. *J. Polym. Sci. Polym. Phys.* **1993**, *31*, 1383–1393.
- (65) Jariyavidyanont, K.; Janke, A.; Androsch, R. Crystal self-nucleation in polyamide 11. *Thermochim. Acta* **2019**, *677*, 139–143.
- (66) Markiewicz, P.; Goh, M. C. Simulation of atomic force microscope tip-sample/sample-tip reconstruction. *J. Vac. Sci. Technol., B: Microelectron. Nanometer Struct.–Process., Meas., Phenom.* **1995**, *13*, 1115–1118.
- (67) Zia, Q.; Androsch, R. Effect of atomic force microscope tip geometry on the evaluation of the crystal size of semicrystalline polymers. *Meas. Sci. Technol.* **2009**, *20*, 097003.
- (68) Hoffman, J. D.; Lauritzen, J. I., Jr. Crystallization of bulk polymers with chain folding: theory of growth of lamellar spherulites. *J. Res. Natl. Bur. Stand. Section A, Phys. Chem.* **1961**, *65*, 297–336.
- (69) Roe, R.-J. *Methods of X-ray and neutron scattering in polymer science*; Oxford University Press, 2000.